Robust high order integral equation solvers for electromagnetic scattering in complex geometries

Zydrunas Gimbutas

Courant Institute of Mathematical Sciences
New York University

gimbutas@cims.nyu.edu

November 29, 2012

Overview

This is joint work with

- James Bremer (U. California, Davis)
- Charles L. Epstein (U. Pennsylvania)
- Leslie Greengard (Courant Institute, NYU)
- Andreas Kloeckner (Courant Institute, NYU)
- Michael O'Neil (Courant Institute, NYU)
- Felipe Vico (Polytechnic University of Valencia, Spain)
- Bogdan Vioreanu (U. Michigan)

Applications: Scattering in complex geometry

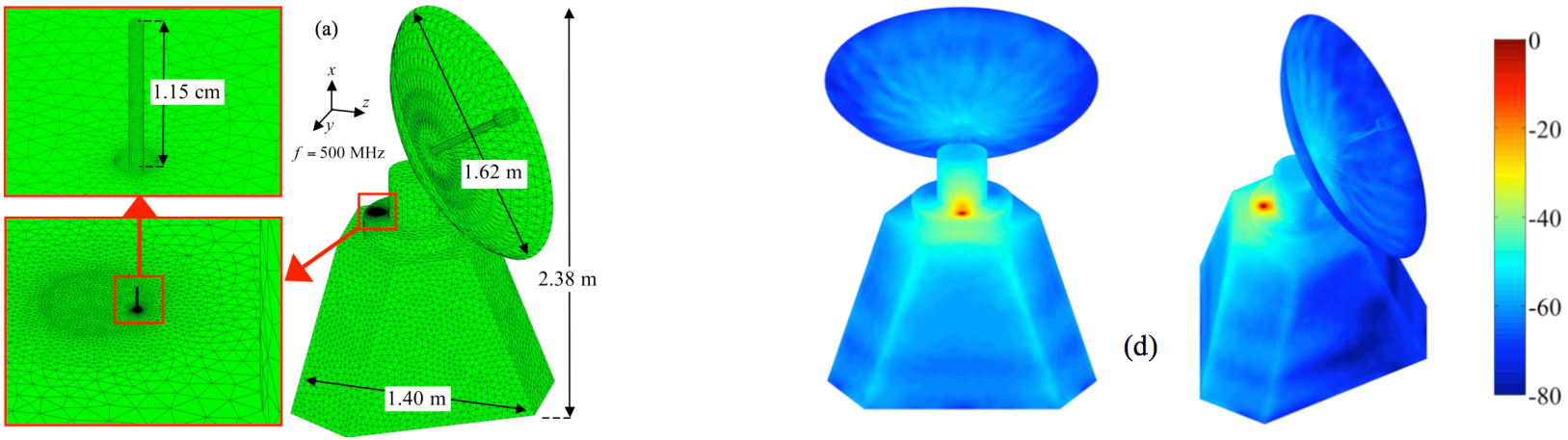

Electromagnetic compatibility problems, antenna design.
Michielsen (U. Michigan)

Applications: Metamaterial design

Transmission through 200 nanorod pairs in a 225 square wavelength box.

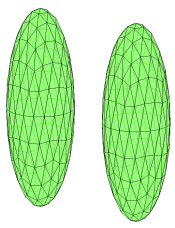

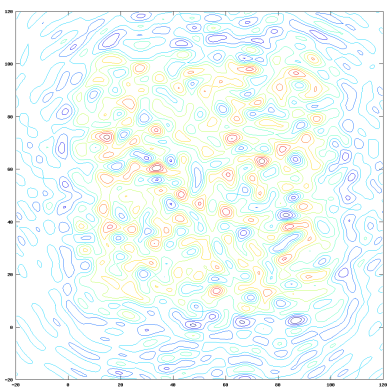

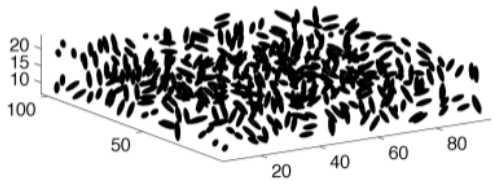

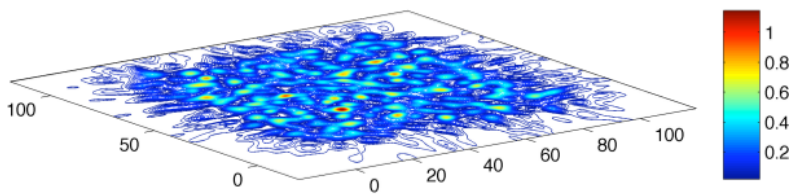

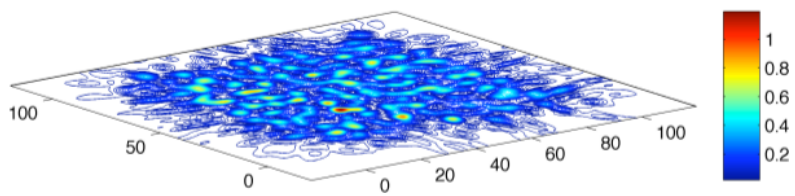

Each ellipsoid is approx. 25x25x75 nm.
In each ellipsoid pair, the centers are separated by 40nm.
Solution time: minutes for each frequency on a single CPU workstation.

Outline of talk

- Classical integral representations for Maxwell's equations
- Spurious resonances and "low-frequency breakdown"
- Augmented charge-current integral equations
- High order discretization of surfaces and solution densities
- Singular layer potentials and quadratures for local interactions
- Numerical experiments

The Maxwell's equations

- A classical problem in electromagnetics concerns the scattering of waves from an obstacle. In the time-harmonic case, the electric and magnetic fields are given by

$$\mathcal{E}(\mathbf{x}, t) = \mathbf{E}(\mathbf{x})e^{-i\omega t}, \quad \mathcal{H}(\mathbf{x}, t) = \mathbf{H}(\mathbf{x})e^{-i\omega t}. \tag{1}$$

The Maxwell's equations

- A classical problem in electromagnetics concerns the scattering of waves from an obstacle. In the time-harmonic case, the electric and magnetic fields are given by

$$\mathcal{E}(\mathbf{x}, t) = \mathbf{E}(\mathbf{x})e^{-i\omega t}, \quad \mathcal{H}(\mathbf{x}, t) = \mathbf{H}(\mathbf{x})e^{-i\omega t}. \tag{1}$$

- In regions free of charge/current, the spatial components satisfy the time-harmonic Maxwell's equations:

$$\nabla \times \mathbf{H} = -i\omega\varepsilon\mathbf{E}, \quad \nabla \times \mathbf{E} = i\omega\mu\mathbf{H}, \tag{2}$$

$$\nabla \cdot \varepsilon\mathbf{E} = 0, \quad \nabla \cdot \mu\mathbf{H} = 0. \tag{3}$$

where ε, μ are permittivity, permeability of exterior region Ω.

The Maxwell's equations: Scattering theory

In electromagnetic scattering, the total field $\{\mathbf{E}^{tot}, \mathbf{H}^{tot}\}$ is generally written as a sum

$$\mathbf{E}^{tot}(\mathbf{x}) = \mathbf{E}^{in}(\mathbf{x}) + \mathbf{E}^{scat}(\mathbf{x}), \quad \mathbf{H}^{tot}(\mathbf{x}) = \mathbf{H}^{in}(\mathbf{x}) + \mathbf{H}^{scat}(\mathbf{x}), \quad (4)$$

where $\{\mathbf{E}^{in}, \mathbf{H}^{in}\}$ describe a known incident field and $\{\mathbf{E}^{scat}, \mathbf{H}^{scat}\}$ denote the scattered field of interest.

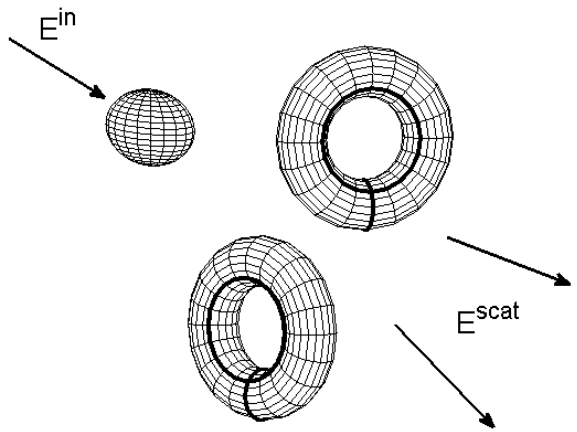

The Maxwell's equations: Vector and scalar potentials

The integral representations for the scattered electromagnetic field $\{\mathbf{E}(\mathbf{x}), \mathbf{H}(\mathbf{x})\}$ are based on classical vector and scalar potentials

$$\mathbf{E}(\mathbf{x}) = i\omega\mathbf{A}(\mathbf{x}) - \nabla\phi(\mathbf{x}), \quad \mathbf{H}(\mathbf{x}) = \frac{1}{\mu}\nabla \times \mathbf{A}(\mathbf{x}), \tag{5}$$

where

$$\mathbf{A}(\mathbf{x}) = \mu \int_\Gamma g_k(\mathbf{x}-\mathbf{y})\mathbf{J}(\mathbf{y})dA_\mathbf{y}, \tag{6}$$

$$\phi(\mathbf{x}) = \frac{1}{\varepsilon} \int_\Gamma g_k(\mathbf{x}-\mathbf{y})\rho(\mathbf{y})dA_\mathbf{y}, \tag{7}$$

$g_k(\mathbf{x}) = e^{ik|\mathbf{x}|}/4\pi|\mathbf{x}|$ is the Green's function for the scalar Helmholtz equation, Γ is the boundary, $k = \omega\sqrt{\varepsilon\mu}$, with the continuity condition

$$\nabla \cdot \mathbf{J}(\mathbf{x}) = i\omega\rho(\mathbf{x}). \tag{8}$$

The Maxwell's equations: Dyadic Green's functions

By incorporating the continuity condition into the integral representations

$$\mathbf{E}(\mathbf{x}) = i\omega\mu \int_{\Gamma} \left[\bar{\mathbf{I}} + \frac{\nabla\nabla}{k^2}\right] g_k(\mathbf{x}-\mathbf{y})\mathbf{J}(\mathbf{y})dA_{\mathbf{y}}, \tag{9}$$

$$\mathbf{H}(\mathbf{x}) = \nabla \times \int_{\Gamma} g_k(\mathbf{x}-\mathbf{y})\mathbf{J}(\mathbf{y})dA_{\mathbf{y}}, \tag{10}$$

we obtain the electric and magnetic dyadic Green's functions

$$\bar{\mathbf{G}}_e(\mathbf{x},\mathbf{y}) = \left[\bar{\mathbf{I}} + \frac{\nabla\nabla}{k^2}\right] g_k(\mathbf{x}-\mathbf{y}), \tag{11}$$

$$\bar{\mathbf{G}}_m(\mathbf{x},\mathbf{y}) = \nabla \times \bar{\mathbf{G}}_e(\mathbf{x},\mathbf{y}) = \nabla \times g_k(\mathbf{x}-\mathbf{y}). \tag{12}$$

The Maxwell's equations: Boundary conditions

- For a perfect conductor, the boundary conditions to be enforced are:

$$\mathbf{n} \times \mathbf{E}^{tot} = 0, \quad \mathbf{n} \cdot \mathbf{H}^{tot} = 0, \tag{13}$$

$$\mathbf{n} \times \mathbf{H}^{tot} = \mathbf{J}, \quad \mathbf{n} \cdot \mathbf{E}^{tot} = \frac{\rho}{\varepsilon}. \tag{14}$$

The Maxwell's equations: Boundary conditions

- For a perfect conductor, the boundary conditions to be enforced are:

$$\mathbf{n} \times \mathbf{E}^{tot} = 0, \quad \mathbf{n} \cdot \mathbf{H}^{tot} = 0, \tag{13}$$

$$\mathbf{n} \times \mathbf{H}^{tot} = \mathbf{J}, \quad \mathbf{n} \cdot \mathbf{E}^{tot} = \frac{\rho}{\varepsilon}. \tag{14}$$

- For uniqueness, with $Im(k) \geq 0$, we assume that the solution satisfies the Sommerfeld (Silver-Muller) radiation condition:

$$\lim_{\mathbf{r} \to \infty} |\mathbf{r}| \left[\mathbf{H}^{scat}(\mathbf{r}) \times \frac{\mathbf{r}}{|\mathbf{r}|} - \sqrt{\frac{\varepsilon}{\mu}} \mathbf{E}^{scat}(\mathbf{r}) \right] = 0. \tag{15}$$

The EFIE and MFIE (Maue)

- The electric field integral equation (EFIE) solves for the unknown current $\mathbf{J}$ by enforcing $\mathbf{n} \times \mathbf{E}^{tot} = 0$. It involves a hypersingular operator acting on $\mathbf{J}$:

$$i\omega\mu\mathbf{n} \times \int_{\Gamma} \left[\bar{\mathbf{I}} + \frac{\nabla\nabla}{k^2}\right] g_k(\mathbf{x}-\mathbf{y})\mathbf{J}(\mathbf{y})dA_{\mathbf{y}} = -\mathbf{n} \times \mathbf{E}^{inc}(\mathbf{x}).$$

- The magnetic field integral equation (MFIE) solves for the unknown current $\mathbf{J}$ by enforcing $\mathbf{n} \times \mathbf{H}^{tot} = \mathbf{J}$.
- There exists a set of frequencies $\{\omega_j\}$ for which the integral equations are not invertible - i.e. *spurious resonances*.

The Combined Field Integral Equation

- The CFIE (and CSIE) were introduced in the 1970's by Harrington, Miller, Mautz, Poggio and others. It avoids spurious resonances by taking a complex linear combination of the EFIE and the MFIE
- Not a Fredholm equation of the second kind
- Other approaches (Yaghjian, ...)

Preconditioners

- Adams and Contopanagos *et al.* made use of the fact that the composition of the hypersingular EFIE operator with itself equals the sum of the identity operator and a compact operator. Leads to CFIE that is resonance-free.
- Christiansen & Nédélec, Colton & Kress, Bruno & Elling & Paffenroth & Turc, Andriulli & Cools & Bagci & Olyslager & Buffa & Christiansen & Michielssen have designed Calderon-based strategies for the EFIE and CFIE.
- Implementation of these schemes rather involved (interaction with corners and edges)

Low frequency breakdown

In the Maxwell system, a separate problem stems from the representation of the electric field itself:

$$\mathbf{E}^{scat} = i\omega\mathbf{A} - \frac{1}{i\omega\varepsilon}\nabla \int_\Gamma g_k(\mathbf{x}-\mathbf{y})(\nabla\cdot\mathbf{J})(\mathbf{y})dA_\mathbf{y}.$$

Numerical discretization as $\omega \to 0$ leads to loss of accuracy, generally referred to as "low-frequency breakdown".

Low frequency breakdown

The usual remedy for low frequency breakdown involves the use of specialized basis functions in the discretization of the current, such as the "loop and tree" method of Wilton and Glisson.

This is a kind of discrete surface Helmholtz decomposition of a piecewise linear approximation of $\mathbf{J}$.

As the frequency goes to zero, the irrotational and solenoidal discretization elements become uncoupled, avoiding the scaling problem that causes loss of precision.

Auxiliary variables

An alternative is to introduce electric charge ρ as an additional variable (Scharstein, Taskinen, Yla-Oijala, Chew).

$$\phi(\mathbf{x}) = \frac{1}{\varepsilon} \int_\Gamma g_k(\mathbf{x} - \mathbf{y}) \rho(\mathbf{y}) dA_\mathbf{y}$$

as well as the continuity condition

$$\nabla \cdot \mathbf{J} = i\omega\rho.$$

This avoids low-frequency breakdown, but is now a Fredholm integral equation subject to a differential-algebraic constraint.

Robust high-fidelity solvers for the Maxwell's equations

- Well-conditioned second kind integral formulations: spurious-resonance free, with localized spectra for better GMRES convergence
- Remove differential-algebraic constraints and hypersingular operators in integral formulations and field postprocessing
- High order description of surfaces and solution densities
- High order quadrature schemes for singular layer potentials
- Fast $O(N)$ or $O(N \log N)$ solvers based on FMM acceleration

Augmented integral equations

- We introduce electric charge ρ as an additional variable and simultaneously impose conditions

$$\mathbf{n} \times \mathbf{H}^{tot} = \mathbf{J}, \quad \mathbf{n} \cdot \mathbf{E}^{tot} = \frac{\rho}{\varepsilon}. \tag{16}$$

- Using the standard jump relations, we obtain a system of linear equations (the electric current-charge integral equation, ECCIE):

$$\begin{aligned} \frac{1}{2}\mathbf{J} - K[\mathbf{J}] &= \mathbf{n} \times \mathbf{H}^{inc}, \\ \frac{\rho}{2} + S'_k[\rho] - i\omega\varepsilon \mathbf{n} \cdot \mathbf{A}[\mathbf{J}] &= \mathbf{n} \cdot (\varepsilon \mathbf{E}^{inc}), \end{aligned}$$

where

$$K[\mathbf{J}](\mathbf{x}) = \mathbf{n} \times \int_\Gamma \bar{\mathbf{G}}_m(\mathbf{x}, \mathbf{y}) \mathbf{J}(\mathbf{y}) dA_\mathbf{y}, \quad S'_k[\rho](\mathbf{x}) = \mathbf{n} \cdot \nabla \int_\Gamma g_k(\mathbf{x}, \mathbf{y}) \rho(\mathbf{y}) dA_\mathbf{y}.$$

Augmented integral equations

- Vico, G-, Greengard, Ferrando-Bataller:
  Let $(\mathbf{J}, \rho)$ be the solution of the ECCIE at a non-resonant frequency ω, and let $\{\mathbf{E}^{inc}, \mathbf{H}^{inc}\}$ satisfy the Maxwell's equations in the neighborhood of Ω. Then $\nabla \cdot \mathbf{J} = i\omega\rho$.

Augmented integral equations

- Vico, G-, Greengard, Ferrando-Bataller:
  Let $(\mathbf{J}, \rho)$ be the solution of the ECCIE at a non-resonant frequency ω, and let $\{\mathbf{E}^{inc}, \mathbf{H}^{inc}\}$ satisfy the Maxwell's equations in the neighborhood of Ω. Then $\nabla \cdot \mathbf{J} = i\omega\rho$.
- For an arbitrary right hand side, the continuity condition is necessary in order for $\{\mathbf{E}^{scat}, \mathbf{H}^{scat}\}$ to satisfy the Maxwell's equations. Existing charge-current formulation incorporate this constraint in one form or another.

Outline of proof

- Taking the surface divergence of the tangential boundary condition $\mathbf{n} \times \mathbf{H}^{tot} = \mathbf{J}$, we have:

$$\nabla \cdot \mathbf{J} - \nabla \cdot (\mathbf{n} \times \mathbf{H}) = \nabla \cdot (\mathbf{n} \times \mathbf{H}^{inc}),$$

$$\nabla \cdot \mathbf{J} + \mathbf{n} \cdot (\nabla \times \mathbf{H}) = -\mathbf{n} \cdot (\nabla \times \mathbf{H}^{inc}),$$

$$\nabla \cdot \mathbf{J} - \mathbf{n} \cdot (i\omega\varepsilon\mathbf{E}) = \mathbf{n} \cdot (i\omega\varepsilon\mathbf{E}^{inc}).$$

Using the standard integral representation for $\mathbf{E}$,

$$\nabla \cdot \mathbf{J} - \mathbf{n} \cdot (i\omega\varepsilon\mathbf{A}[\mathbf{J}] - \nabla S_k[\nabla \cdot \mathbf{J}]) = \mathbf{n} \cdot (i\omega\varepsilon\mathbf{E}^{inc}).$$

Augmented integral equations

- Dividing by $i\omega$, and taking the limit to the boundary, we have

$$\frac{1}{2}\frac{\nabla \cdot \mathbf{J}}{i\omega} + S_k'\left[\frac{\nabla \cdot \mathbf{J}}{i\omega}\right] - \mathbf{n} \cdot i\omega\varepsilon\mathbf{A}[\mathbf{J}] = \mathbf{n} \cdot (\varepsilon\mathbf{E}^{inc}). \qquad (17)$$

- Recall that the second equation of the ECCIE was:

$$\frac{\rho}{2} + S_k'[\rho] - \mathbf{n} \cdot i\omega\varepsilon\mathbf{A}[\mathbf{J}] = \mathbf{n} \cdot (\varepsilon\mathbf{E}^{inc}).$$

- Therefore, the solution $(\mathbf{J}, \rho)$ of the ECCIE satisfies the continuity condition $\nabla \cdot \mathbf{J} = i\omega\rho$.

Augmented integral equations

- Dividing by $i\omega$, and taking the limit to the boundary, we have

$$\frac{1}{2}\frac{\nabla \cdot \mathbf{J}}{i\omega} + S_k'\left[\frac{\nabla \cdot \mathbf{J}}{i\omega}\right] - \mathbf{n} \cdot i\omega\varepsilon\mathbf{A}[\mathbf{J}] = \mathbf{n} \cdot (\varepsilon\mathbf{E}^{inc}). \qquad (17)$$

- Recall that the second equation of the ECCIE was:

$$\frac{\rho}{2} + S_k'[\rho] - \mathbf{n} \cdot i\omega\varepsilon\mathbf{A}[\mathbf{J}] = \mathbf{n} \cdot (\varepsilon\mathbf{E}^{inc}).$$

- Therefore, the solution $(\mathbf{J}, \rho)$ of the ECCIE satisfies the continuity condition $\nabla \cdot \mathbf{J} = i\omega\rho$.
- At zero frequency, the equation (17) has a null-space, corresponding to the interior Neumann problem for the Laplace equation.

Augmented integral equations

- The solution can be made unique by enforcing that the total charge is equal to zero.

$$\frac{1}{2}\rho + S_k'[\rho] - \mathbf{n}\cdot i\omega\varepsilon\mathbf{A}[\mathbf{J}] = \mathbf{n}\cdot(\varepsilon\mathbf{E}^{inc}), \tag{18}$$

$$\int_\Gamma \rho(\mathbf{y})dA_\mathbf{y} = 0. \tag{19}$$

- The rank-1 correction trick:

$$S_k'[\rho](\mathbf{x}) = \mathbf{n}(\mathbf{x})\cdot\nabla_\mathbf{x}\int_\Gamma g_k(\mathbf{x}-\mathbf{y})\rho(\mathbf{y})dA_\mathbf{y} \rightarrow$$

$$\int_\Gamma \left[\mathbf{n}(\mathbf{x})\cdot\nabla_\mathbf{x} g_k(\mathbf{x}-\mathbf{y}) + 1\right]\rho(\mathbf{y})dA_\mathbf{y}. \tag{20}$$

- Useful for dealing with near singular cases.

Low frequency breakdown: near field

- The dyadic electric Green's function for **E** field:

$$\mathbf{E}(\mathbf{x}) = i\omega\mu \int_{\Gamma} \left[\bar{\mathbf{I}} + \frac{\nabla\nabla}{k^2}\right] g_k(\mathbf{x}-\mathbf{y})\mathbf{J}(\mathbf{y}) dA_{\mathbf{y}}, \qquad (21)$$

  is replaced with the charge-current representation:

$$\mathbf{E}(\mathbf{x}) = i\omega\mu \int_{\Gamma} g_k(\mathbf{x}-\mathbf{y})\mathbf{J}(\mathbf{y}) dA_{\mathbf{y}} - \nabla \int_{\Gamma} g_k(\mathbf{x}-\mathbf{y})\rho(\mathbf{y}) dA_{\mathbf{y}}. \qquad (22)$$

Low frequency breakdown: near field

- The dyadic electric Green's function for **E** field:

$$\mathbf{E}(\mathbf{x}) = i\omega\mu \int_\Gamma \left[\bar{\mathbf{I}} + \frac{\nabla\nabla}{k^2}\right] g_k(\mathbf{x}-\mathbf{y})\mathbf{J}(\mathbf{y})dA_\mathbf{y}, \qquad (21)$$

  is replaced with the charge-current representation:

$$\mathbf{E}(\mathbf{x}) = i\omega\mu \int_\Gamma g_k(\mathbf{x}-\mathbf{y})\mathbf{J}(\mathbf{y})dA_\mathbf{y} - \nabla \int_\Gamma g_k(\mathbf{x}-\mathbf{y})\rho(\mathbf{y})dA_\mathbf{y}. \qquad (22)$$

- Vector and scalar potential parts decouple at low frequencies.

Low frequency breakdown: far field

- The far field **E** signature:

$$\mathbf{E}_{\infty}^{\hat{\alpha}}(\hat{\mathbf{x}}) = \hat{\alpha} \cdot \int_{\Gamma} e^{ik\hat{\mathbf{x}}\cdot\mathbf{y}} \mathbf{J}(\mathbf{y}) dA_{\mathbf{y}}, \tag{23}$$

where $\hat{\mathbf{x}}$ is a unit vector in the $\mathbf{x}$ direction and $\hat{\alpha}$ is the angular polarization of the receiver. For small ω, the far field signature $\mathbf{E}_{\infty}^{\hat{\alpha}}$ is of the order $O(\omega)$, while $\mathbf{J}$ is $O(1)$.

Low frequency breakdown: far field

- The far field **E** signature:

$$\mathbf{E}_{\infty}^{\hat{\alpha}}(\hat{\mathbf{x}}) = \hat{\alpha} \cdot \int_{\Gamma} e^{ik\hat{\mathbf{x}}\cdot\mathbf{y}} \mathbf{J}(\mathbf{y}) dA_{\mathbf{y}}, \tag{23}$$

  where $\hat{\mathbf{x}}$ is a unit vector in the $\mathbf{x}$ direction and $\hat{\alpha}$ is the angular polarization of the receiver. For small ω, the far field signature $\mathbf{E}_{\infty}^{\hat{\alpha}}$ is of the order $O(\omega)$, while $\mathbf{J}$ is $O(1)$.

- In $(\mathbf{J}, \rho)$ representation, all terms are of the order $O(\omega)$:

$$\mathbf{E}_{\infty}^{\hat{\alpha}}(\hat{\mathbf{x}}) = \hat{\alpha} \cdot \int_{\Gamma} \left[e^{ik\hat{\mathbf{x}}\cdot\mathbf{y}} - 1 \right] \mathbf{J}(\mathbf{y}) dA_{\mathbf{y}} - i\omega\hat{\alpha} \cdot \int_{\Gamma} \mathbf{y}\rho(\mathbf{y}) dA_{\mathbf{y}}. \tag{24}$$

Low frequency breakdown

- Vico, Gimbutas, Greengard, Ferrando-Bataller, "Overcoming Low-Frequency Breakdown of the Magnetic Field Integral Equation", to appear in IEEE Transactions on Antennas and Propagation.

Augmented integral equations

Integral formulations using the second set of boundary conditions

$$\mathbf{n} \times \mathbf{E}^{tot} = 0, \quad \mathbf{n} \cdot \mathbf{H}^{tot} = 0, \tag{25}$$

lead to the augmented electric field integral equations:

$$\begin{aligned} \mathbf{n} \times i\omega\mu \int_\Gamma g_k(\mathbf{x}-\mathbf{y})\mathbf{J}(\mathbf{y})dA_\mathbf{y} - \mathbf{n} \times \nabla \int_\Gamma g_k(\mathbf{x}-\mathbf{y})\rho(\mathbf{y})dA_\mathbf{y} &= -\mathbf{n} \times \mathbf{E}^{inc}, \\ \mathbf{n} \cdot \nabla \times \int_\Gamma g_k(\mathbf{x}-\mathbf{y})\mathbf{J}(\mathbf{y})dA_\mathbf{y} &= -\mathbf{n} \cdot \mathbf{H}^{inc}. \end{aligned}$$

The off-diagonal blocks are Hilbert (Riesz) operators.
Currently very active research area: charge-current formulations (Taskinen, Yla-Oijala), generalized Debye integral equations (Epstein, Greengard), etc.

Discretization schemes

- Classical integral representations for Maxwell's equations
- Spurious resonances and "low-frequency breakdown"

- Augmented charge-current integral equations

- High order discretization of surfaces and solution densities
- Singular layer potentials and quadratures for local interactions

Discretization of singular layer potentials

The numerical schemes for discretizing the ECCIE and augmented EFIE require accurate evaluation of the following singular layer potentials:

$$\mathbf{n} \times \int_\Gamma \bar{\mathbf{G}}_m(\mathbf{x},\mathbf{y})\mathbf{J}(\mathbf{y})dA_\mathbf{y}, \quad \mathbf{n} \cdot \nabla \int_\Gamma g_k(\mathbf{x},\mathbf{y})\rho(\mathbf{y})dA_\mathbf{y},$$
$$\int_\Gamma g_k(\mathbf{x}-\mathbf{y})\mathbf{J}(\mathbf{y})dA_\mathbf{y}, \quad -\mathbf{n} \times \nabla \int_\Gamma g_k(\mathbf{x}-\mathbf{y})\rho(\mathbf{y})dA_\mathbf{y},$$
$$\mathbf{n} \cdot \nabla \times \int_\Gamma g_k(\mathbf{x}-\mathbf{y})\mathbf{J}(\mathbf{y})dA_\mathbf{y},$$

and good representations for the scatterer Γ, solution $(\mathbf{J}, \rho)$ and incoming field $\{\mathbf{E}^{inc}, \mathbf{H}^{inc}\}$.

Surface descriptors

- In the simplest geometric model, the surface of the scatterer Γ is approximated by a collection of flat triangles.
- On each triangle, there are two linearly independent tangent directions t_1 and t_2.
- The unknown electric currents $\mathbf{J}$ and charge ρ on each triangle are defined by $\mathbf{J}_1 t_1 + \mathbf{J}_2 t_2$ and ρ, respectively, and the electromagnetic fields are evaluated at the triangle centroids.

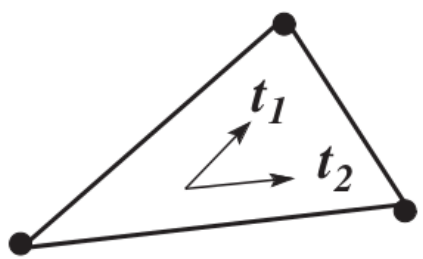

Surface descriptors

- Flat triangulations with constant densities: single layer potentials are accurate to $O(h^2)$, double layer potentials - $O(h)$, hypersingular ...
- Very slow convergence rates; codes are hard to test
- Limited choice of useful integral representations

- At least quadratic surface patches are needed

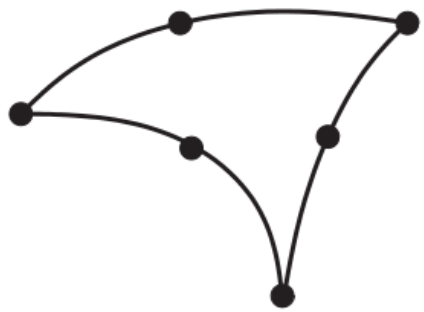

- Cubic and high order surface patches!
- Interfacing with CAD packages

Solution discretization

- To represent current and charge densities, we use high order Gaussian-like interpolation/quadrature rules for smooth functions on triangles, Rokhlin-Vioreanu.
- These are also the collocation nodes (selected in the interior of each patch) where we evaluate the electromagnetic fields and impose the boundary conditions.

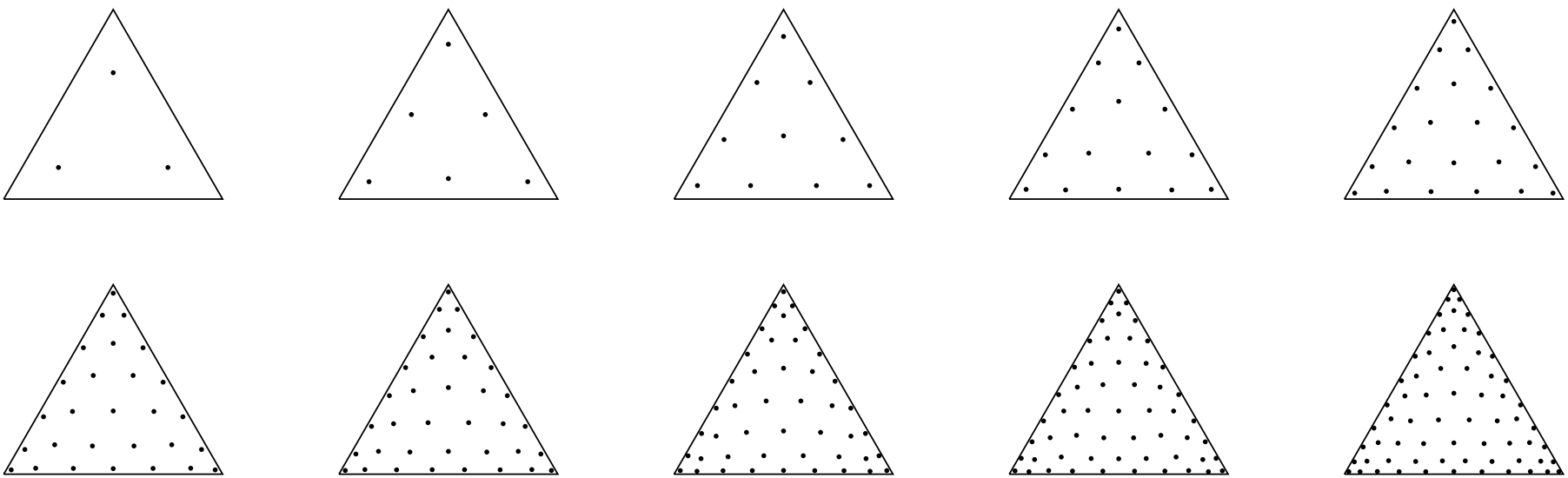

Solution discretization

The nodes are fully symmetric, well-conditioned, and the corresponding quadrature weights are positive.

interp	0	1	2	3	4	5	6	7	8	9	10
quadr	1	2	4	5	7	8	10	12	14	15	17
nodes	1	3	6	10	15	21	28	36	45	55	66
cond #	1.0	1.0	1.4	1.9	2.1	3.4	4.3	4.8	4.8	6.5	8.1

The table contains the degree of intepolation, the degree of quadrature, the number of nodes, and the condition number of interpolation process for R.-V. nodes up to degree 10.

Arbitrary degree rules are available.

Quadratures for weakly singular and p.v. layer potentials

Numerical evaluation of integral operators on smoothly parametrized surfaces (J. Bremer, G-):

$$S_k[f](\mathbf{x}) = \int_\Gamma g_k(\mathbf{x}-\mathbf{y}) f(\mathbf{y}) dA_\mathbf{y}, \tag{26}$$

$$S_k'[f](\mathbf{x}) = \mathbf{n}(\mathbf{x}) \cdot \nabla_\mathbf{x} \int_\Gamma g_k(\mathbf{x}-\mathbf{y}) f(\mathbf{y}) dA_\mathbf{y}, \tag{27}$$

$$D_k[f](\mathbf{x}) = \int_\Gamma \mathbf{n}(\mathbf{y}) \cdot \nabla_\mathbf{y} g_k(\mathbf{x}-\mathbf{y}) f(\mathbf{y}) dA_\mathbf{y}, \tag{28}$$

$$R_k[f](\mathbf{x}) = \mathbf{t}(\mathbf{x}) \cdot \nabla_\mathbf{x} \int_\Gamma g_k(\mathbf{x}-\mathbf{y}) f(\mathbf{y}) dA_\mathbf{y}, \tag{29}$$

$$R_k^*[f](\mathbf{x}) = \int_\Gamma \mathbf{t}(\mathbf{y}) \cdot \nabla_\mathbf{y} g_k(\mathbf{x}-\mathbf{y}) f(\mathbf{y}) dA_\mathbf{y}. \tag{30}$$

Quadratures for weakly singular and p.v. layer potentials

- Γ is subdivided into curved triangular patches Γ_i.
- Density f is represented as a piece-wise smooth function on Γ.
- Singular integrals are evaluated on R.-V. interpolation nodes $\mathbf{x}_t = \mathbf{x}(u_j, v_j)$:

$$S_k[f](\mathbf{x}_t) = \int_{\Gamma_i} g_k(\mathbf{x}_t - \mathbf{y}) f(\mathbf{y}) dA_{\mathbf{y}} \tag{31}$$

via auxiliary quadrature nodes $\mathbf{y}_s^{aux} = \mathbf{y}(u_s, v_s)$:

$$S_k[f](\mathbf{x}_t) = \sum_s w_s g_k(\mathbf{x}_t - \mathbf{y}_s^{aux}) f(\mathbf{y}_s^{aux}) |A(\mathbf{y}_s^{aux})|, \tag{32}$$

where w_s are the auxiliary quadrature weights and $|A|$ is the surface area element.

Quadratures for weakly singular and p.v. layer potentials

- The auxiliary quadratures strongly depend on the locations of interpolation nodes in R^3 and the stretching factors of patches Γ_i.
- The number of auxiliary quadrature nodes is approximately of the order 1000–2000; we use a set of precomputed tables for up-to 20th degree polynomials.

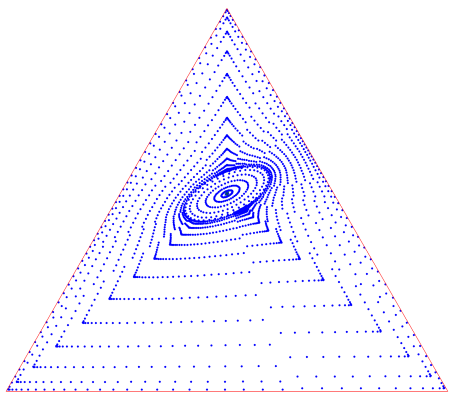
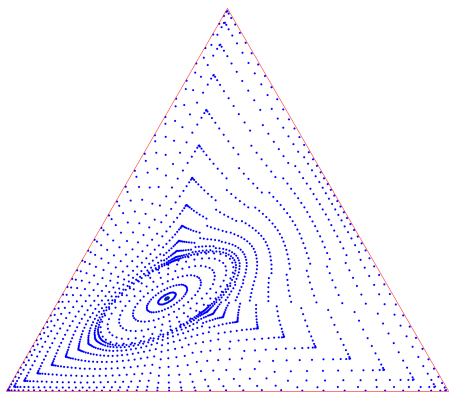
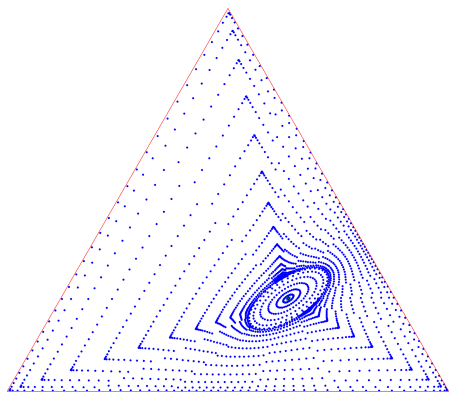

Quadratures for weakly singular and p.v. layer potentials

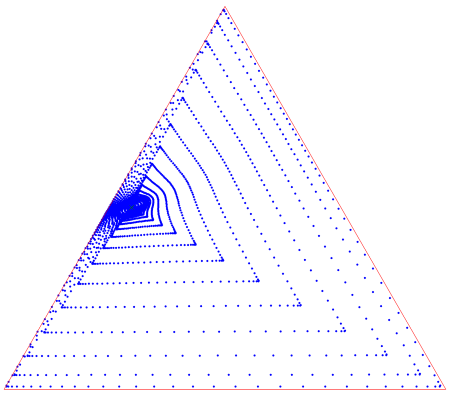
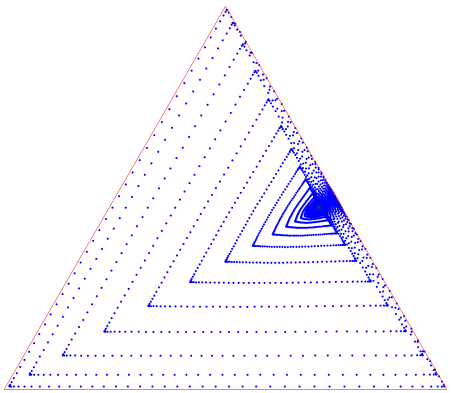
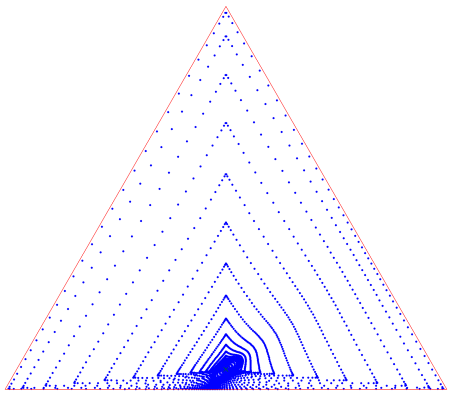
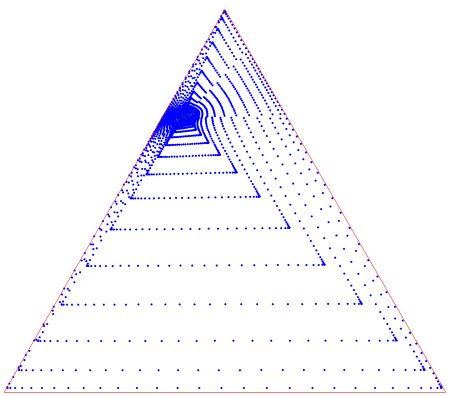
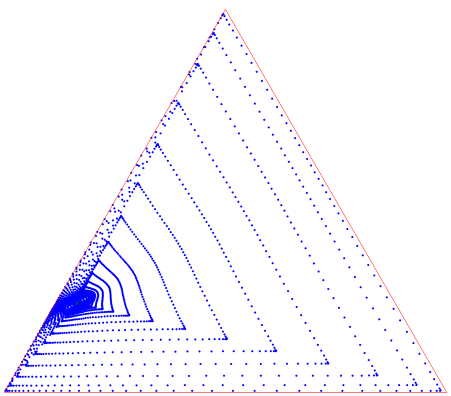
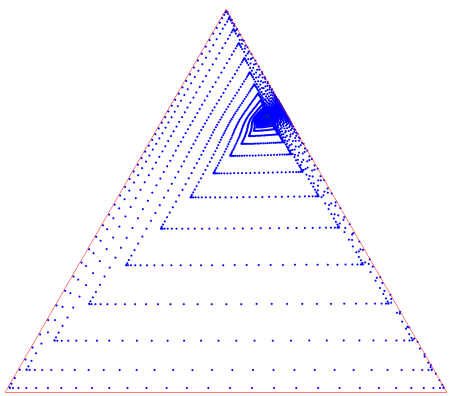

The number of auxiliary quadrature nodes is roughly the same for all interpolation points.

Numerical experiments

- Classical integral representations for Maxwell's equations
- Spurious resonances and "low-frequency breakdown"
- Augmented charge-current integral equations
- High order discretization of surfaces and solution densities
- Singular layer potentials and quadratures for local interactions
- Numerical experiments

Accuracy testing

How do we test these codes?

- Generate a known solution due to an electromagnetic source (electric dipole, plane wave, . . .)
- Grab $\{\mathbf{E}^{test}, \mathbf{H}^{test}\}$ on the surface Γ and use as data
- Solve the integral equation for $(\mathbf{J}, \rho)$
- Compare $\{\mathbf{E}, \mathbf{H}\}$ to known $\{\mathbf{E}^{test}, \mathbf{H}^{test}\}$ inside the conductor

We use the total field extinction theorem, which is due to the inhomogeneous boundary conditions

$$\mathbf{n} \times \mathbf{H}^{tot} = \mathbf{J}, \quad \mathbf{n} \cdot \mathbf{E}^{tot} = \frac{\rho}{\varepsilon}. \tag{33}$$

Numerical results: Smooth geometries

The ECCIE:
$\mathbf{n} \times \mathbf{H}^{tot} = \mathbf{J}, \mathbf{n} \cdot \mathbf{E}^{tot} = \rho, k = 1$

N_{tri}	N_{disc}	N_{sys}	E_{sph}
12	540	1620	5.92E-05
48	2160	6480	5.46E-09
192	8640	25920	1.85E-12

8th order convergence tests
45 points/triangle

The augmented EFIE:
$\mathbf{n} \times \mathbf{E}^{tot} = 0, \mathbf{n} \cdot \mathbf{E}^{tot} = \rho, k = 1$

N_{tri}	N_{disc}	N_{sys}	E_{sph}
12	540	1620	1.01E-02
48	2160	6480	4.41E-05
192	8640	25920	8.11E-07

8th order convergence tests
45 points/triangle

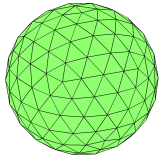

sphere

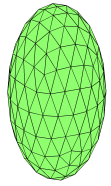

ellipsoid

Numerical experiments: Singular geometries

The Helmholtz equation (exterior Neumann boundary condition).

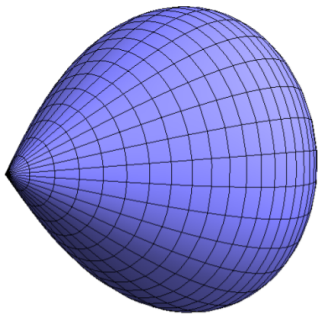

$$x(s,t) = 2\sin(t/2),$$
$$y(s,t) = -\cos(s)\sin(t),$$
$$z(s,t) = \sin(s)\sin(t),$$
$$0 \leq t \leq \pi, 0 \leq s \leq 2\pi.$$

N_{tri}	N_{disc}	N_{sys}	E_{sph}
4	180	180	1.52E-03
16	720	720	2.42E-05
64	2880	2880	1.04E-07
256	11520	11520	9.09E-10
1024	46080	46080	7.04E-13

8th order convergence tests
45 points/triangle

The domain is discretized using an adaptive mesh, (Bremer)
Recompression schemes, (Bremer, Helsing)

Numerical experiments

- Fully resolved EM simulations
  - 10,000-100,000 of discretization nodes for simple objects
  - Millions of points for complex geometries

- Corners and edges
  - Adaptive mesh refinement
  - Recompression schemes (Bremer, Helsing)

Numerical results

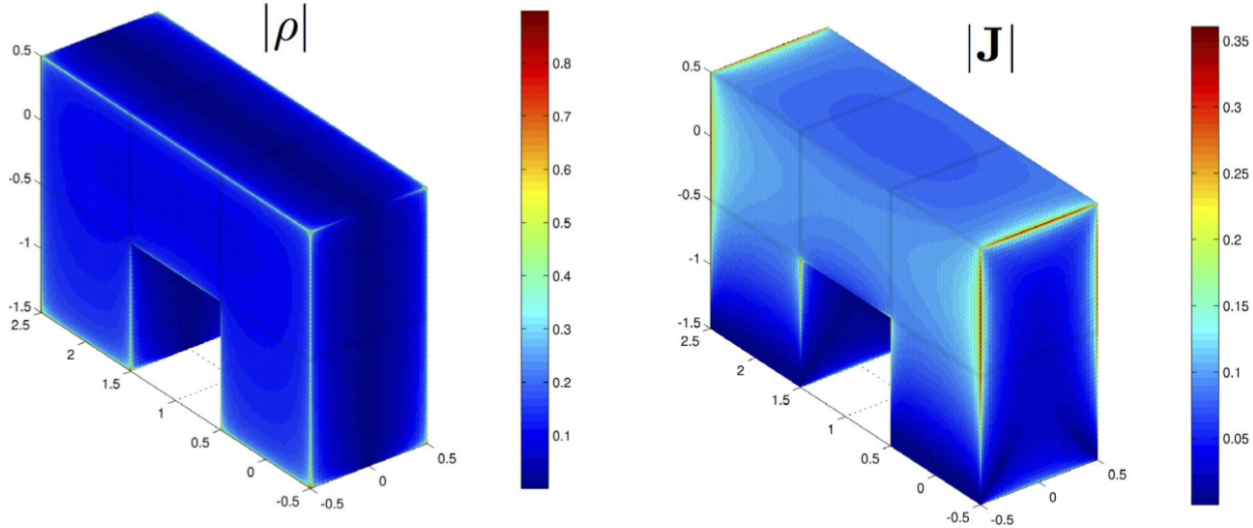

The solution of the MFIE (current **J**) is plotted on the right. The solution of the scalar equation in the ECCIE formulation yields the charge density ρ, plotted on the left. The arch is constructed from the concatenation of five cubes - each of which is discretized using an adaptive mesh refined toward the edges. The wavenumber (k) was set to 1, and the direction of incidence was along the z-axis with E polarized along the x-axis.

Future Work

- Fast layer potential evaluation tools (FMM acceleration)
- Coupling to CAD tools: quadratic and higher order patches
- Singular densities: corner and edge compressors
- Integral representations with localized spectra
- Integral representations for surfaces with complicated topology
- Integration into variety of application codes: antennas on complex platforms, MRI, metamaterial design

Thanks

- AFOSR MURI Grant FA9550-06-1-0337,
- Courant Mathematics and Computing Laboratory,
- DoD NSSEFF Program Award FA9550-10-1-0180.